Available online at www.pelagiaresearchlibrary.com

Pelagia Research Library

Der Chemica Sinica, 2017, 8(3):355-364

ISSN : 0976-8505
CODEN (USA): CSHIA5

Synthesis, Quantum Chemical Studies and Cytotoxicity Activity of Diastereoselective trans-2,3-dihydronaphtho[2,3-b]furan Derivatives

Sivalingam Lakshmanan*, Narayanan Ramalakshmi and S Arul Antony

Post-Graduate and Research Department of Chemistry, Presidency College, Chennai-05, Tamil Nadu, India

ABSTRACT

A green, one-pot three component approach for the synthesis of diastereoselective trans-2,3-dihydronaphtho [2,3-b] furan derivatives(4a-g). Synthesized compounds were evaluated for their anticancer activity against A549 human lung adenocarcinoma cancer cell line. Among all the tested Compounds 4b and 4c showed the most potent biological activity against A549 lung cancer cell line. Docking simulation was performed to position compounds 4b and 4c showed greater affinity for anaplastic lymphoma kinase (ALK) receptor. Quantum chemical studies were carried out on these compounds to understand the structural features essential for activity using DFT/6-31G level of theory.

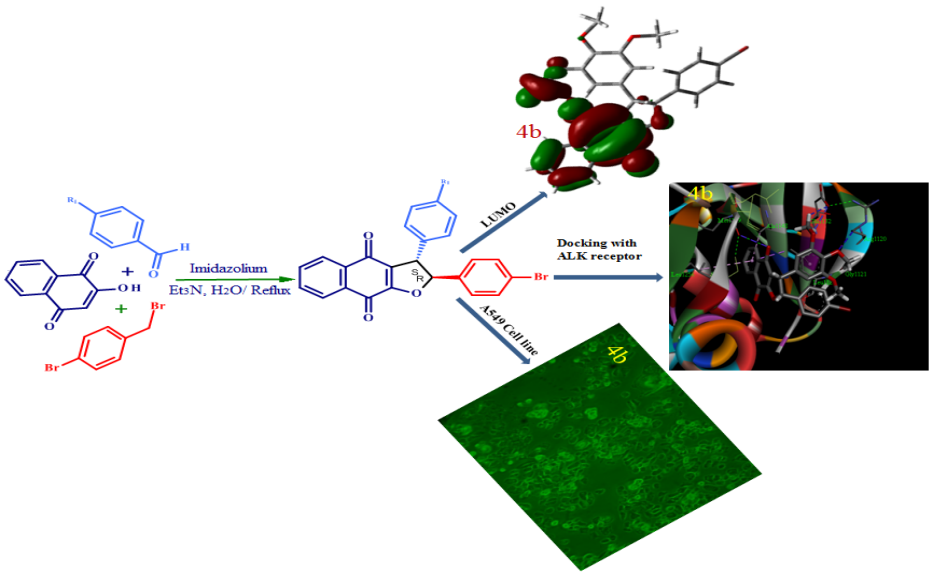

Graphical abstract

Keywords: One-pot, 2,3-dihydronaphtho[2,3-b]furan, Cytotoxicity, Molecular docking, DFT

INTRODUCTION

Cancer is one of the important contributors to deaths worldwide, corresponding to almost 1600 deaths per day in the United States. Lung cancer is a leading cause of cancer death accounting for approximately 26% of all female and 28% of all male cancer deaths in 2013 [1]. Among the anti-cancer strategies chemotherapy is available with drugs/ chemicals which interfere with cell division, inhibit tumour angiogenesis or induce cancer cell death by various signalling pathways but have potential harm to normal cells [2-4]. However, it should be noted that many types of cancer develop resistance to chemotherapeutic drugs [5]. Therefore, the research of anti-cancer drugs with better activity and fewer side effects is becoming increasingly active.

Anaplastic lymphoma kinase (ALK) is a receptor tyrosine kinase (RTK) belonging to the insulin receptor superfamily, which includes insulin-like growth factor-1 receptor (IGF-1R) and leukocyte tyrosine kinase (LTK). A variety of ALK inhibitors have been developed and examined in clinical trials, such as alectinib, ceritinib, crizoitnib. Among them, crizotinib (Xalkori) was the first small molecule inhibitor which was approved as a treatment of NSCLC including ALK fusion gene, EML4-ALK by FDA in 2011 [6,7]. Although crizotinib was very efficient for the treatment of ALK-positive NSCLC harboring ALK rearrangements [8,9], acquired drug resistance caused by point-mutations of ALK has been identified in patients treated with crizotinib [10,11]. The most abundant expression of ALK occurs in the neo-natal brain, suggesting a possible role for ALK in early brain development [12]. As a result, the selective inhibition of ALK emerged as an attractive target for cancer therapies [13,14].

Naphthoquinones (NQs) have been the subject of much research owing to their pharmacological activities [15,16], antiallergic [17], antibacterial [18,19], anti-neoplastic [20], antifungal [21], anti-hypoxic [22], antithrombotic [23,24] antiplatelet [25], antiviral [26,27], antiischemic [28], apoptosis [29,30], and Anticancer activity has also been reported for the 1,4-Naphthoquinones [31-34]. As continuation of our synthetic efforts to develop biologically important of 1,4-Naphthoquinones derivatives [35], molecular docking and DFT method is play an significant role in development of drug design [36,37].

MATERIALS AND METHODS

All of the chemicals used in the synthesis were purchased from Sigma-Aldrich and were used as received. Melting points were measured in open capillary tubes and are uncorrected. The ^{1}H-NMR, ^{13}C-NMR were recorded on a Bruker (Avance) 300 MHz NMR instrument using TMS as an internal standard and DMSO as a solvent. Standard Bruker software was used throughout. Chemical shifts are given in parts per million (δ-scale) and the coupling constants are given in Hertz. Silica gel-G plates (Merck) were used for TLC analysis with a mixture of petroleum ether (60-80^{o}C) and ethyl acetate as the eluent. ESI mass was recorded using a Thermo Fleet-LC mass instrument.

General procedure for the synthesis of 2, 3-dihydronaphtho [2, 3-b]furan-4,9-dione

To a mixture of 10 mol% Et_3N, 2-hydroxy-1,4-naphthoquinone (1mmol), Aromatic aldehyde (1mmol) and Phenacyl bromide (1 mmol), N-methyl Imidzolium (1mmol) in water (10 ml) was refluxed for 180 min at 90^{0}C. After completion of the reaction (indicated by TLC), the free-flowing solid was filtered and washed with ethanol (10 ml) to afford the desired products as yellow solid without column chromatography in good yield.

2-(4-bromophenyl)-3-(4-chlorophenyl)-2,3-dihydronaphtho[2,3-b]furan-4,9-dione (4a)

Yellow solid, M. P: 242-244ºC. ^{1}H NMR (300 MHz, DMSO): δ (ppm) δ 7.98 -7.50 (m, 4H), 7.42 (d, J=8.6 Hz, 2H), 7.32 (d, J=8.6 Hz, 2H), 7.02 (dd, J=5.2 Hz, 4H), 5.66 (d, J=5.0 Hz, 1H), 4.57 (d, J=5.2 Hz, 1H); ^{13}C NMR (75 MHz, DMSO, TMS): δ (ppm) δ 182.61, 179.76, 149.61, 138.27, 131.27, 128.87, 126.14, 124.17, 123.25, 78.73, 52.21, 49.39, 42.12. ESI-MS (M+1); Calcd. for $C_{24}H_{14}BrClO_3$; 465.98. Found 466.52.

2-(4-bromophenyl)-2,3-dihydro-3-(3,4,5-trimethoxyphenyl)naphtho[2,3-b]furan-4,9-dione (4b)

Yellow solid, M. P: 232-234ºC. ^{1}H NMR (300 MHz, DMSO): δ (ppm) 7.89-7.44 (m, 4H), 7.11(s, 2H), 7.08-6.98 (m, 4H), 5.66 (d, J=5.1 Hz, 1H), 4.57 (d, J=5.2 Hz, 1H), 3.66(s, 9H). ^{13}C NMR (75 MHz, DMSO, TMS): δ (ppm) 183.71, 179.65, 141.09, 140.65, 138.67, 131.78, 129.87, 127.54, 125.77, 124.65, 118.78, 84.45, 41.98, 30.77. ESI-MS (M+1); Calcd. for $C_{27}H_{21}BrO_6$; 520.05. Found 521.65.

2-(4-bromophenyl)-3-(4-(dimethylamino)phenyl)-2,3 dihydronaphtho[2,3-b]furan-4,9-dione (4c)

Yellow solid, M. P.: 226-228ºC. ^{1}H NMR (300 MHz, DMSO): δ (ppm) 7.85-7.79 (m, 4H), 7.66 (d, J=4.8 Hz, 2H), 7.14 (d, J=8.6 Hz, 2H), 6.70 (d, J=8.6 Hz, 2H), 6.35 (d, J=5.2 Hz, 2H), 5.24 (d, J=5.1 Hz, 1H), 4.69 (d, J=5.2 Hz, 1H), 2.88 (s, 6H). ^{13}C NMR (75 MHz, DMSO, TMS): δ (ppm) 183.98, 175.24, 154.73, 145.99, 133.92, 133.50, 132.6, 132.13, 131.28, 130.56, 128.56, 120.97, 113.11, 80.95, 55.28, 48.57. ESI-MS (M+1); Calcd. for $C_{26}H_{20}BrNO_3$; 473.06 Found 473.98.

2-(4-bromophenyl)-2,3-dihydro-3-(4-hydroxyphenyl)naphtho[2,3-b]furan-4,9-dione (4d)

Yellow solid, M. P: 214-216ºC. ^{1}H NMR (300 MHz, DMSO): δ (ppm) 8.58 (s, 1H), 7.85-7.81 (m, 4H), 7.69-7.68 (d, J=3.6 Hz, 2H), 7.16-7.14 (d, J=8.4 Hz, 2H), 6.75-6.73 (d, J=8.4 Hz, 2H), 6.36-6.34 (d, J=5.4 Hz, 2H), 5.25 (d, J=5.2 Hz, 1H), 4.74 (d, J=5.2 Hz, 1H). ^{13}C NMR (75 MHz, DMSO, TMS): δ (ppm) 182.54, 174.98, 156.63, 152.83, 140.71, 136.25, 135.47, 134.51, 134.16, 130.97, 129.65, 129.02, 122.65, 118.72, 83.91, 54.03. ESI-MS (M+1); Calcd. for

$C_{24}H_{15}BrO_4$; 446.02 Found 447.38.

3-(5-bromo-2-hydroxyphenyl)-2-(4-bromophenyl)-2,3-dihydronaphtho [2,3-b]furan-4,9-dione (4e)

Yellow solid, M. P: 232-234ºC. ^{1}H NMR (300 MHz, DMSO): δ (ppm) 8.91-8.90 (d, 2H), 7.66 (d, J=4.8 Hz, 2H), 7.14 (d, J=8.6 Hz, 2H), 6.70 (d, J=8.6 Hz, 2H), 6.35 (d, J=5.2 Hz, 2H), 5.24 (d, J=5.8 Hz, 1H), 4.69 (d, J=5.2 Hz, 1H), 2.88 (s, 6H). ^{13}C NMR (75 MHz, DMSO, TMS): δ (ppm) 183.02, 177.34, 158.91, 148.47, 130.99, 130.96, 130.71, 130.68, 130.56, 130.21, 127.85, 126.20, 118.68, 81.76, 52.26. ESI-MS (M+1); Calcd. for $C_{24}H_{14}Br_2O_4$; 523.93 Found 524.89.

2-(4-bromophenyl)-2,3-dihydro-3-(4-nitrophenyl)naphtho[2,3- *b*]furan-4,9-dione (4f)

Yellow solid, M. P: 246-248ºC. ^{1}H NMR (300 MHz, DMSO): δ (ppm) 7.84 -7.80 (m, 4H), 7.67-7.66 (d, J=4.8 Hz, 2H), 7.30- 7.28 (d, J=8.7 Hz, 2H), 6.65-6.62 (d, J=8.8 Hz, 2H), 6.36-6.35 (d, J=5.0 Hz, 2H), 5.25 (d, J=5.2 Hz, 1H), 4.69 (d, J=5.2 Hz, 1H). ^{13}C NMR (75 MHz, DMSO, TMS): δ (ppm) 183.63, 176.84, 147.21, 139.47, 136.52, 136.49, 135.78, 132.87, 131.43, 126.14, 124.17, 123.25, 121.45, 120.78, 118.23, 79.85, 52.21. ESI-MS (M+1); Calcd. for $C_{24}H_{14}BrNO_5$; 475.01 Found 476.84.

2-(4-bromophenyl)-2,3-dihydro-3-(3,4-dimethoxyphenyl)naphtho[2,3-b]furan-4,9-dione (4g)

Yellow solid, M. P: 228-230ºC. ^{1}H NMR (300 MHz, DMSO): δ (ppm) 7.85-7.79 (m, 4H), 7.66 (d, J=4.8 Hz, 2H), 7.14 (d, J=8.6 Hz, 2H), 6.70 (d, J=8.6 Hz, 2H), 6.65 (s,1H), 5.24 (d, J=5.0 Hz, 1H), 4.69 (d, J=5.2 Hz, 1H), 3.69 (s, 6H). ^{13}C NMR (75 MHz, DMSO, TMS): δ (ppm) 182.46, 179.85, 158.32, 144.29, 141.03, 136.84, 133.54, 131.78, 129.87, 128.65, 127.54, 125.77, 124.65, 118.78, 84.45, 59.73, 41.98. ESI-MS (M+1); Calcd. for $C_{26}H_{19}BrO_5$; 490.04 Found 491.65.

Cell culture

The human lung (A459) cell lines were purchased from the National Centre for Cell Science (Pune, India). Cell culture protocols method by following the procedure reported by Leland Booth et al. [38].

Cytotoxicity studies

The Cytotoxicity towards human lung (A459) cancer cells were analyzed using drugs 5-FU as a control as-synthesized compounds 4a-g with the 3-(4,5-dimethylthiazol-2-yl)-2,5-diphenyltetrazolium bromide (MTT) examine and Fluorouracil as reference drug. Testing was carried out in 96- well cell culture plate (1X104cells/well). Subsequently, culture plates were incubated for one day with 10 µM of as-synthesized compounds 4a-g. After that, MTT solution was supplementary on culture well. Following one day incubation, the culture medium restrain unreached MTT was detached charily and calculated at optical microscope (570 nm).

Molecular docking

To investigate the potential binding mode of inhibitors, all the compounds were subjected to molecular docking using the AUTODOCK 1.5.6 docking program. Because of the critical roles of aberrant Signalling in cancer, anaplastic lymphoma kinase (ALK) receptor is an attractive oncology target for therapeutic intervention. To this end, the X-ray crystal structure of ALK in complex with crizotinib was downloaded from the protein data bank (PDBID: 2XP2) and was used for the docking study. Ligand 2D structures were drawn using ChemDraw Ultra 8.0. Chem3D Ultra 8.0 was used to convert 2D structure into 3D and the energy minimized using semi-empirical MM2 method. Minimize energy to minimum RMS gradient of 0.100 was set in each iteration. All structures were saved as .pdb file format for input to Auto Dock-Tools (ADT) version 1.5.6. All the ligand structures were then saved in PDBQT file format, for input into AUTODOCK version 4.2.

For the molecular docking study, protein structure was obtained from the Protein Data Bank; the ALK structure PDB ID was 2XP2. The co-crystallized ligand (crizotinib) in the ALK structure was removed. For the protein structure, all hydrogen atoms were added, lower occupancy residue structures were deleted, and any incomplete side chains were replaced using the ADT version 1.5.6. Further ADT was used to remove crystal water, added Gagteiger charges to each atom, and merged the non-polar hydrogen atoms to the protein structure. The structures were then saved in PDBQT file format, for input into AUTODOCK version 1.5.4. A grid box with dimension of 60 × 60 60 Å3 with 0.886 spacing and centred on 38.083, 46.914, 17.164 was created around the binding site of crizotinib on ALK protein using Auto Dock Tools. The centre of the box was set at crizotinib and grid energy calculations were carried out. For the AUTODOCK docking calculation, default parameters were used and 10 docked conformations were generated for each compound, the energy calculations were done using genetic algorithms. Docking of different ligands to protein was performed using AUTODOCK, same protocols used in as that of validation study. All docking were taken into

2.5 million energy evaluations were performed for each of the test molecules. Docked ligand conformations were analyzed in terms of energy, hydrogen bonding, and hydrophobic interaction between ligand and receptor protein ALK. Detailed analyses of the ligand–receptor interactions were carried out, and final coordinates of the ligand and receptor were saved as pdb files. Docked structures were visualized using Discovery Studio Visualizer 2.5 (Accelrys Software Inc.). The free energy of binding (FEB) of all compounds were calculated.

RESULTS AND DISCUSSION

Chemistry

The trans-2,3-dihydronaphtho[2,3-b] furan derivatives were synthesized (**Scheme 1**, **Table 1**) as previously reported with some modification [39]. A plausible mechanistic explanation for this one - pot multicomponent reaction starts with a Knoevenagel condensation between 2-hydroxy-1,4-naphthoquinone (1 mm) and substituted aldehyde (1 mm) to form the intermediate. The next step is a Michael addition of Imidazolium ylide with enones affords the zwitterionic intermediate and SN_2 substitution reaction followed by cyclization to affords the stereoselective formation of trans -2,3-dihydronaphtho [2,3-b] furan-4,9-dione titled product. The structures of the prepared titled products were fully characterized by ^1H NMR spectra of 4a, the two protons at 2,3-position of dihydrofuran ring exhibit two doublets at 4.5 and 5.6ppm with the vicinal coupling constant J=4.8 Hz. The similar peak pattern and coupling constant less than 6.0 Hz were also seen in the other 1H NMR spectra of prepared 2,3-dihydronaphtho[2,3-b]furan-4,9 -dione derivatives. It has been established that in cis-2,3-dihydrofuran the vicinal coupling constant of the two methine protons J=7-10 Hz, while in trans-2,3-dihydrofuran vicinal coupling constant J=4-7Hz [40] which result trans-isomer is thermodynamically more stable than cis isomer is also agreement with lower heat of formation, as estimated using DFT/B3LYP:6-31G calculations [41] **Table 2**.

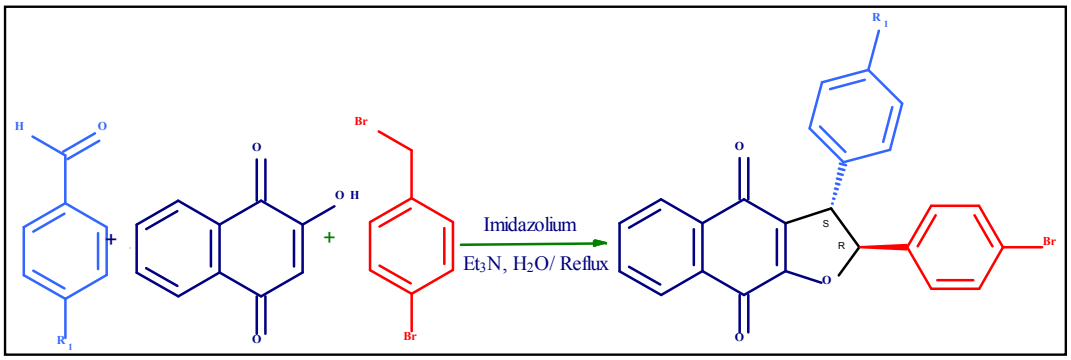

Scheme 1: Synthesis of trans-2,3-dihydronaphtho[2,3-b]furan derivatives.

Table 1: Biological target of trans-2,3-dihydronaphtho[2,3-b]furan derivatives (4a-g).

Entry	Compounds	R_1	Yield (%)
1	4a	4-ClC_6H_4	73
2	4b	3,4,5-$(OMe)_3C_6H_2$	78
3	4c	4-$N(Me)_2C_6H_4$	64
4	4d	4-OHC_6H_4	72
5	4e	5-Br,2-OHC_6H_3	79
6	4f	4-$NO_2C_6H_4$	82
7	4g	3,4-$(OMe)_2C_6H_3$	70

Table 2: Physicochemical parameters of compound 2-(4-bromophenyl)-2,3-dihydro-3-(4-nitrophenyl) naphtha [2,3-b]furan-4,9-dione.

4e	$E_{total\ (kcal)}$ HF	$\mu_{(Debye)}$	HOMO	LUMO	HLG
CIS	-6365.9523	6.7711	-0.14817	-0.13067	0.0175
TRANS	-6366.1381	7.5424	-0.15615	-0.13410	0.02205

Biological Evaluation

Cytotoxicity activity

In the present work, we investigated the biological effects of a series of trans- 2,3-dihydronaphtho [2,3-b] furan derivatives to determine their mechanism of action in human lung cancer cell line A549. The cytotoxicity of the as-synthesized compounds (4a-g) evaluated against A549 cells. The compounds 4b, 4c and 4e had obvious cytotoxicity, whereas other compounds had not so much effect at 10 μM concentration. The majority of compounds at 5 and 10 μM exhibited anti-proliferation effects on A549 cells. Consequently, the trans-2,3-dihydronaphtho[2,3-b]furan derivatives suppressed the growth of A549 cells in dose. Moreover, compounds 4b, 4c and 4e exhibited more significant cytotoxicity and the inhibitory rate was almost up to 70-80% equivalent to 5-FU. Our finding demonstrated that all tested derivatives exhibited considerable cell growth inhibition at concentrations 10 μM, in which compounds 4b, 4c and 4e exerted optimal results and the others modest anti-proliferation efficiency (**Figure 1**), there by IC_{50} of the compounds were totally less than 10 μM (**Table 3**). Therefore, we selected 5 and 10 μM concentration for the following investigation according to the results of cell viability. Percent of cell viability was calculated and the inhibition of growth of human lung cancer cell line is defined by the nature of the substituent. The compounds having electron donating of three methoxy or methyl group 4b and 4c exhibited significant cytotoxic activity with IC_{50} values having 4.01 and 4.69 μM against promising therapeutic agents for A549 lung adenocarcinoma cancer cell line.

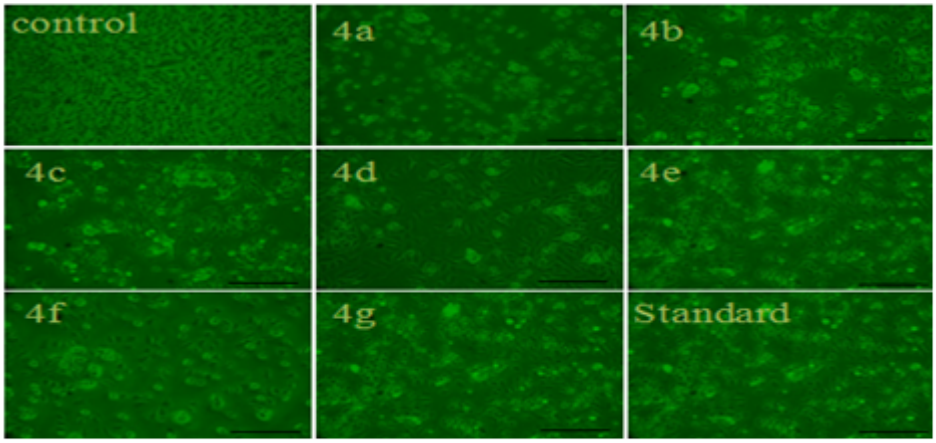

Figure 1: Phase contrast images of as synthesized compounds (4a-4g) treated A549 cell.

Table 3: IC_{50} and FEB values of compounds 4a–g.

Compounds	IC_{50}(μM)	FEB[a] (kcal/mol)	No. of H Bonds
4a	8.92 ± 2.02	-7.42	2
4b	4.01 ± 0.07	-8.95	5
4c	4.69 ± 0.09	-8.91	1
4d	15.36 ± 1.08	-7.63	1
4e	6.06 ± 0.03	-8.21	2
4f	18.59 ± 1.07	-7.38	3
4g	10.02 ± 1.09	-7.82	4
5-FUb	6.02 ± 0.04	-	-
[a] = Free energy binding, [b] = Fluorouracil used as a positive control.			

Molecular docking

Synthesized compounds 4b, 4c and 4e show very high binding energy with the ALK receptor which exposed similarity with the cytotoxic activity of among all the tested derivatives. The most active compound 4b has a very high binding energy value -8.95 kcal/mol exhibited H- bonding with Met1199, Glu1132, Arg1120, Gly1121 and hydrophobic interaction with Leu1256, Ala1148, Leu1122 which results five hydrogen bonds with ALK receptor (**Figure 2a**) and also compounds 4c, has equal binding energy value -8.91kcal/mol and interact with amino acids namely Ser1206, Leu122, Pro1260, Glu1210 (**Figure 2b**). The moderate active Compounds 4e has a very high binding energy value

-8.21kcal/mol and interact with amino acids namely Gln1146, Leu1145, (**Figure 2c**). Interestingly, electron donating substituted compounds exhibit higher binding energy values compare with other groups decreased the binding energy, for example compound 4f shows low binding energy value -7.38 kcal/ mol in presence of electron withdrawing substituted (**Figure 2d**).The order of binding affinity of docked trans-2,3-dihydronaphtho[2,3-b] furan derivatives against the ALK receptor is 4b>4c>4e>4g> 4d>4a> and 4f with the range of binding energy being -8.95 to -7.38 kcal/ mol (**Table 3**). The numbers of hydrogen bonds vary from one to five with most key interacting residues, Leu1122 actively participate in the formation of hydrophobic bonding with the compounds 4b, 4c and 4e are responsible for forming strong bonds between ligands and receptor ALK (2XP2.pdb) to inhibit the function of enzyme and cytotoxic effect.

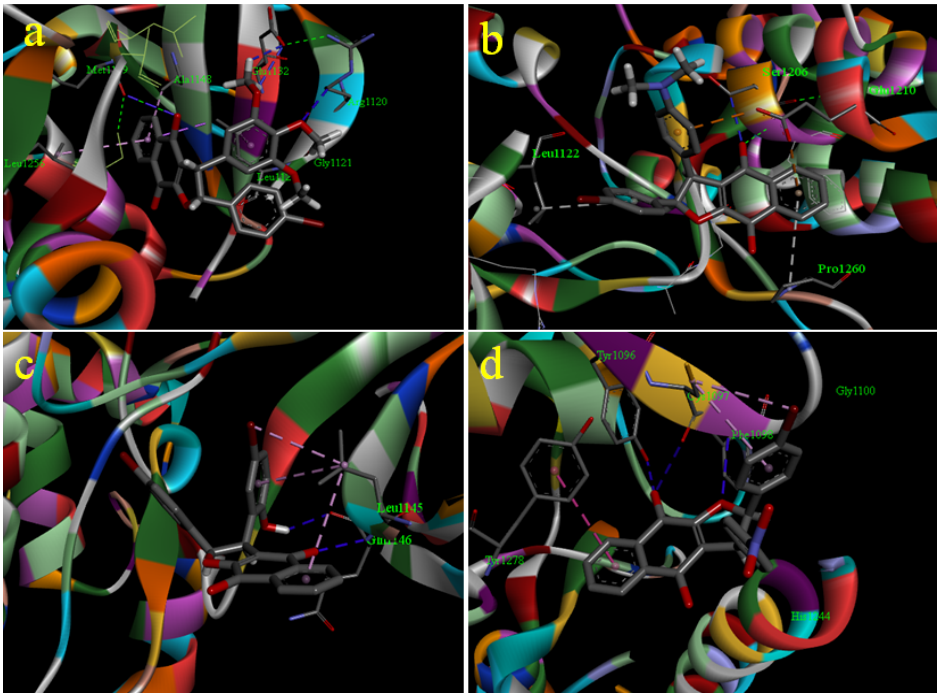

Figure 2: (a) and (b) Binding mode of the most active compound 4b, 4c with ALK receptor, (c) Binding mode of moderate active compound 4e with ALK receptor, (d) Binding mode of least active compound 4f with ALK receptor. The amino acids involved in hydrogen (blue dashed line), hydrophobic (white dashed line) interactions are highlighted.

Table 3: IC_{50} and FEB values of compounds 4a–g.

Compounds	IC_{50}(µM)	FEB[a] (kcal/mol)	No. of H Bonds
4a	8.92 ± 2.02	-7.42	2
4b	4.01 ± 0.07	-8.95	5
4c	4.69 ± 0.09	-8.91	1
4d	15.36 ± 1.08	-7.63	1
4e	6.06 ± 0.03	-8.21	2
4f	18.59 ± 1.07	-7.38	3
4g	10.02 ± 1.09	-7.82	4
5-FUb	6.02 ± 0.04	-	-

[a] = Free energy binding, [b] = Fluorouracil used as a positive control.

Density functional theory (DFT) study

Theoretical calculations were performed by the density functional theory (DFT) method at the B3LYP/ 6-31G level of theory in the Gaussian 03 package of programs [42]. According to the frontier molecular orbital theory, (HOMO) has the priority to provide electrons while LUMO can accept electrons first are the most important factors that affect the bioactivity [43,44]. Higher HOMO energy and lower LUMO energy in the drug molecule result in larger stabilizing

interactions and, hence, binding with the receptor. The orbital energies of both HOMO and LUMO and their gaps were calculated for all the molecules and are reported in **Table 4**. It is remarkable that compounds 4b, 4c, 4e and 4g having the lowest energy gap (ΔE) of 0.686, 0.615, 0.689, and 0.858 ev, respectively, exhibit the highest cytotoxic activity. We also obtained a plot of the HOMO and LUMO of the molecules of each group to analyze the main atomic contributions for these orbitals. The importance of observing these plots was to determine which atoms were located at the possible sites of electronic transfer between the molecule under study and its biological target. The results illustrate that HOMO lobes are spread mainly over substituted aromatic rings; In contrast, the LUMO lobes are almost homogeneously spread over naphthoquinone moiety (**Figure 3**). Molecular electrostatic potential (MEP) mapped surface of the molecules are calculated by DFT/ B3LYP/6-31G method at the 0.02 isovalues and 0.0004 density values. Molecular electrostatic potential and electrostatic potential are the useful quantities to display the charge distributions of molecules are used to visualize variably charged regions of a molecule. The electrostatic potential is used to find the reactive site of a molecule. Red represents regions of most electro negative electrostatic potential, blue represents regions of most positive electrostatic potential (**Figure 4**).

Table 4: Energies of both HOMO and LUMO and their gaps (in ev) calculated for all compounds.

Comp.	$E_{total\ (kcal)}$ E_{HF}	$\mu_{(Debye)}$	E_{HOMO}	E_{LUMO}	ΔE
4a	-4179.9504	5.5066	-6.316	-3.824	2.492
4b	-4062.8723	5.1512	-4.129	-3.443	0.686
4c	-3853.9979	3.6909	-3.821	-3.206	0.615
4d	-3795.5612	4.1154	-5.873	-3.712	2.160
4e	-6366.1381	7.5424	-4.402	-3.713	0.689
4f	-3924.7824	7.8895	-6.805	-3.993	2.811
4g	-3948.9678	3.8487	-4.581	-3.721	0.858

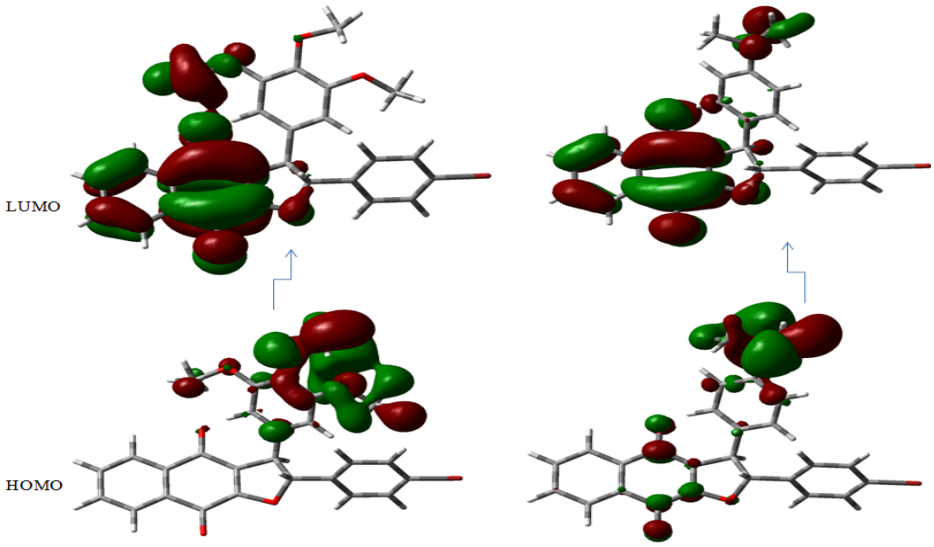

Figure 3: Plots of the HOMO and LUMO density map of compounds 4b (left) and 4c (right).

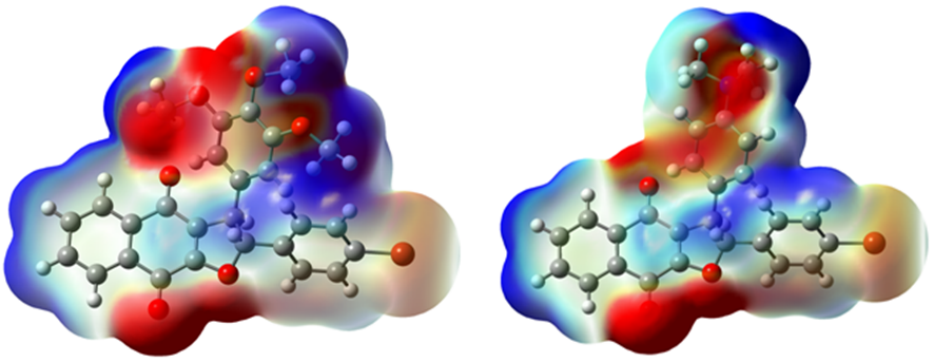

Figure 4: Electrostatic potential mapping on the electron density of 4b and 4c.

CONCLUSION

In summary, theoretical quantum-chemical calculations correlate well with modern research related to trans-2,3-dihydronaphtho[2,3-b] furan derivatives (4a-g). This result also supports its higher activities and investigated their biological activities against human lung cancer cell line A549 *in vitro*. The results indicated that the as-synthesized compounds showed significant anticancer activities. Among all the compounds screened, 4b, 4c and 4e showed very high activity at 10μM concentration against A549 cell line. Molecular docking of the most potent inhibitor (4a-g) into binding site of ALK was performed, and the results showed compound 4b, 4c and 4e could bind well with the ALK active site.

CONFLICT OF INTEREST

The Authors declare no conflict interest.

REFERENCES

[1] Siegel R, Naishadham D, Jemal A (**2013**) Cancer statistics, 2013. *CA Cancer J Clin* 63: 11-30.

[2] Zheng CY, Lam SK, Li YY, Fong BM, Mak JC, et al. (**2013**) Combination of arsenic trioxide and chemotherapy in small cell lung cancer. *Lung Cancer* 82: 222-230.

[3] Warshamana-Greene GS, Litz J, Buchdunger E, Garcia-Echeverria C, Hofmann F, et al. (**2015**) The insulin-like growth factor-I receptor kinase inhibitor, NVP-ADW742, sensitizes small cell lung cancer cell lines to the effects of chemotherapy. *Clin Cancer Res* 11: 1563-1571.

[4] Zhao J, Miao J, Zhao B, Zhang S, Yin D (**2005**) Safrole oxide inhibits angiogenesis by inducing apoptosis. *Vasc Pharmacol* 43: 69-74.

[5] Kibria G, Hatakeyama H, Harashima H (**2014**) Cancer multidrug resistance: mechanisms involved and strategies for circumvention using a drug delivery system. *Arch Pharm Res* 37: 4-15.

[6] Frampton JE (**2013**) Crizotinib: A Review of Its Use in the Treatment of Anaplastic Lymphoma Kinase-Positive, Advanced Non-Small Cell Lung Cancer. *Drugs* 73: 2031-2051.

[7] Shaw AT, Yasothan U, Kirkpatrick P (**2011**) Crizotinib. *Nat Rev Drug Discov* 10: 897-898.

[8] Ou SH, Bartlett CH, Mino-Kenudson M, Cui J, Iafrate AJ (**2012**) In the second decade of molecular targeted therapy in oncology. *Oncologist* 17: 1351-1375.

[9] Camidge DR, Doebele RC (**2012**) Treating ALK positive lung cancer: Early successes and coming challenges. *Nat Rev Clin Oncol* 9: 268-277.

[10] Zhang S, Wang F, Keats J, Zhu XT, Ning YY, et al. (**2011**) Crizotinib-resistant mutants of EML4-ALK identified through an accelerated mutagenesis screen. *Chem Biol Drug Des* 78: 999-1005.

[11] Ceccon M, Mologni L, Bisson W, Scapozza L, Gambacorti-Passerini C (**2013**) Crizotinib-resistant NPM-ALK mutants confer differential sensitivity to unrelated Alk inhibitors. *Mol Cancer Res* 11: 122-132.

[12] Duyster J, Bai RY, Morris SW (**2001**) Translocations involving anaplastic lymphoma kinase (ALK). *Oncogene* 20: 5623-5637.

[13] Krytska K, Ryles HT, Sano R, Raman P, Infarinato NR, et al. (**2015**) Crizotinib Synergizes with Chemotherapy in Preclinical Models of Neuroblastoma. *Clin Cancer Res* 22: 948-960.

[14] Shaw AT, Solomon B (**2011**) Targeting anaplastic lymphoma kinase in lung cancer. *Clin Cancer Res* 17: 2081-2086.

[15] Wellington KW (**2015**) Understanding cancer and the anticancer activities of naphthoquinones – a review. *RSC Adv* 5: 20309-20338.

[16] Bonifazi EL, Ríos-Luci C, León LG, Burton G, Padrón JM, et al. (**2010**) Antiproliferative activity of synthetic naphthoquinones related to lapachol. First synthesis of 5-hydroxylapachol. *Bioorg Med Chem* 18: 2621-2630.

[17] Huang LJ, Chang FC, Lee KH, Wang JP, Teng CM, et al. (**1998**) Synthesis and antiplatelet, antiinflammatory, and antiallergic activities of substituted 3-chloro-5,8-dimethoxy-1,4-naphthoquinone and related compounds. *Bioorg Med Chem* 6: 2261-2269.

[18] Inbaraj JJ, Chignell CF (**2004**) Cytotoxic action of juglone and plumbagin: a mechanistic study using HaCaT keratinocytes. *Chem Res Toxicol* 17: 55-62.

[19] Huang ST, Kuo HS, Hsiao CL, Lin YL (**2002**) Efficient synthesis of 'redox-switched' naphthoquinone thiol-crown ethers and their biological activity evaluation. *Bioorg Med Chem* 10: 1947-1952.

[20] Gordaliza M, Miguel del Corral J, Angeles Castro M, Mar Mahiques M, Garcia-Gravalos M, et al. (**1996**) Synthesis and bioactivity of new antineoplastic terphenylquinones. *Bioorg Med Chem Lett* 6: 1859-1864.

[21] Tandon VK, Chhor RB, Singh RV, Rai S, Yadav DB (**2004**) Design, synthesis and evaluation of novel 1,4-naphthoquinone derivatives as antifungal and anticancer agents. *Bioorg Med Chem Lett* 14: 1079-1083.

[22] Sasaki K, Abe H, Yoshizaki F (**2002**) In vitro antifungal activity of naphthoquinone derivatives. *Biol Pharm Bull 25:* 669-670.

[23] Jin YR, Ryu CK, Moon CK, Cho MR, Yun YP (**2004**) Inhibitory effects of J78, a newly synthesized 1,4-naphthoquinone derivative, on experimental thrombosis and platelet aggregation. *Pharmacology* 70: 195-200.

[24] Kartoflitskaya AP, Stepanyuk GI, Yushkova VV, Marintsova NG, Novikov VP (**1997**) Synthesis and the anti hypoxic and antiischemic activity of some 2-chloro-1,4-naphthoquinone derivatives. *Pharm Chem J* 31: 291-292.

[25] Yuk DY, Ryu CK, Hong JT, Chung KH, Kang WS, et al. (**2000**) Antithrombotic and antiplatelet activities of 2-chloro-3-[4-(ethylcarboxy)-phenyl]-amino-1,4-naphthoquinone (NQ12), a newly synthesized 1,4-naphthoquinone derivative. *Biochem Pharmacol* 60: 1001-1008.

[26] Ravelo AG, Estévez-Braun A, Chávez-Orellana H, Pérez-Sacau E, Mesa-Siverio D (**2004**) Recent studies on natural products as anticancer agents. *Curr Top Med Chem* 4: 241-265.

[27] Ilina TV, Semenova EA, Pronyaeva TR, Pokrovskii AG, Nechepurenko TV, et al. (**2002**) Inhibition of HIV-1 Reverse Transcriptase by Aryl-Substituted Naphto- and Anthraquinones. *Dokl Biochem Biophys* 382: 56-59.

[28] Kim HJ, Kang SK, Mun JY, Chun YJ, Choi KH, et al. (**2003**) Involvement of Akt in mitochondria-dependent apoptosis induced by a cdc25 phosphatase inhibitor naphthoquinone analog. *FEBS Lett* 555: 217-222.

[29] Richwien A, Wurm G (**2004**) Influence of 2-aryl-3-halogen/3-hydroxy-1,4-naphthoquinones with salicylic and cinnamic acid partial structures on the arachidonic acid cascade. *Pharmazie* 59: 163-169.

[30] Wurm G, Schwandt S (**2003**) Methylated 2-aryl-1,4-naphtoquinone derivatives with diminished antioxidative activity.

[31] Hallak M, Thakur BK, Winn T, Shpilberg O, Bittner S, et al. (**2013**) Induction of death of leukemia cells by TW-74, a novel derivative of chloro-naphthoquinone. *Anticancer Res* 33: 183-190.

[32] da Rocha DR, de Souza AC, Resende JA, Santos WC, dos Santos EA, et al. (**2011**) Synthesis of new 9-hydroxy-α- and 7-hydroxy-β-pyran naphthoquinones and cytotoxicity against cancer cell lines. *Org Biomol Chem* 9: 4315-4322.

[33] Costantino L, Barlocco D (**2006**) Privileged structures as leads in medicinal chemistry. *Curr Med Chem* 13: 65-85.

[34] Pérez-Sacau E, Díaz-Peñate RG, Estévez-Braun A, Ravelo AG, García-Castellano JM, et al. (**2007**) Synthesis and pharmacophore modeling of naphthoquinone derivatives with cytotoxic activity in human promyelocytic leukemia HL-60 cell line. *J Med Chem* 50: 696-706.

[35] Lakshmanan S, Ramalakshmi N (**2016**) One-pot, four-component synthesis of benzylpyrazolyl naphthoquinone derivatives and molecular docking studies. S*ynth Commu* 46: 2045-2052.

[36] Islam N, Pandith AH (**2012**) Modeling of the anti-cancer activity of 1, 4-naphthoquinone derivatives; a theoretical study. *J*

Pharm Res 5: 1846-1853.

[37] Becke AD (**1993**) A new mixing of Hartree–Fock and local density□functional theories. *J Chem Phys* 98: 1372.

[38] Booth JL, Duggan ES, Patel VI, Langer M, Wu W, et al. (**2016**) Bacillus anthracis spore movement does not require a carrier cell and is not affected by lethal toxin in human lung models. *Microbes Infect* 18: 615-626.

[39] Wu ZZ, Jang YJ, Lee CJ, Lee YT, Lin W (**2013**) A versatile and practical method for regioselective synthesis of polysubstituted furanonaphthoquinones. *Org Biomol Chem* 11: 828-834.

[40] Dunlop AP, Hurd CD (**1950**) Base-catalyzed condensation of α-halogenated ketones with β-keto esters. *J Org Chem* 15: 1160-1164.

[41] SM Rajesh, S Perumal, JC Menéndez, S Pandian, R Murugesan (**2012**) Facile ionic liquid-mediated, three-component sequential reactions for the green, regio-and diastereoselective synthesis of furocoumarins. *Tetrahedron* 68: 5631-5636.

[42] MJ Frisch, GW Trucks, HBea Schlegel, GE Scuseria, MA Robb, et al. (**2004**) Gaussian 03, Revision C. 01; Gaussian, Inc., Wallingford, CT, USA.

[43] Schön U, Antel J, Brückner R, Messinger J, Franke R, et al. (**1998**) Synthesis, pharmacological characterization, and quantitative structure-activity relationship analyses of 3,7,9,9-tetraalkylbispidines: derivatives with specific bradycardic activity. *J Med Chem* 41: 318-331.

[44] Roy DR, Pal N, Mitra A, Bultinck P, Parthasarathi R, et al. (**2007**) An atom counting strategy towards analyzing the biological activity of sex hormones. *Eur J Med Chem* 42: 1365-1369.